




Article

Production of SnS₂ Nanostructure as Improved Light-Assisted Electrochemical Water Splitting

Haizeng Song ^{1,2}, Han Wu ^{1,2}, Yuan Gao ³, Ka Wang ³, Xin Su ^{1,2}, Shancheng Yan ^{3,*}  and Yi Shi ^{1,2,*}

¹ Collaborative Innovation Center of Advanced Microstructures, Nanjing University, Nanjing 210093, China

² School of Electronic Science and Engineering, Nanjing University, Nanjing 210093, China

³ School of Geography and Biological Information, Nanjing University of Posts and Telecommunications, Nanjing 210023, China

* Correspondence: yansc@njupt.edu.cn (S.Y.); yshi@nju.edu.cn (Y.S.)

Received: 7 August 2019; Accepted: 28 August 2019; Published: 1 September 2019



Abstract: Tin disulfide (SnS₂) has gained a lot of interest in the field of converting solar energy into chemical fuels in light-assisted electrochemical water splitting due to its visible-light band gap and high electronic mobility. However, further decreasing the recombination rate of electron-hole pairs and increasing the density of active states at the valence band edge of the photoelectrodes were a critical problem. Here, we were successful in fabricating the super-thin SnS₂ nanostructure by a hydrothermal and solution etching method. The super-thin SnS₂ nanostructure as a photo-electrocatalytic material exhibited low overpotential of 0.25 V at the current density of $-10 \text{ mA}\cdot\text{cm}^{-2}$ and the potential remained basically unchanged after 1000 cycles in an H₂SO₄ electrolyte solution, which was better than that of the SnS₂ nanosheet and SnS/SnS₂ heterojunction nanosheet. These results show the potential application of super-thin SnS₂ nanostructure in electrochemical/photo-electrocatalytic field.

Keywords: layered semiconductor; solution etching; SnS₂ nanostructure; light-Assisted electrochemical water splitting

1. Introduction

In recent years, there has been more and more research on the application of two-dimensional (2D) layered materials as field-effect-transistors (FETs) [1,2], photodetectors [3,4], photocatalysis [5], lithium-ion battery, etc. [6–9], which were dependent on the excellent electronic mobility and optical properties [10,11]. Besides, 2D layered materials have also been considered as a photocatalysis to water splitting in the next generation since its 2D conductive channel is beneficial to fast carrier transport and greatly reduce the recombination rate in the photoelectrode, and the larger surface area is conducive to rapid charge transfer and enhance electrochemical reaction at the interface, which could improve the reaction efficiency [12–14]. As an original member of semiconductor metal sulfides family, the hexagonal SnS₂ is nontoxic, inexpensive, chemically stable in acidic and neutral solutions, and visible-light band gap of 2.2–2.4 eV [14–16]. In the last few years, it has been proved to be a promising photocatalyst in the application of dye degradation processes.

Recently, the SnS₂ has been considered as a photo-electric-catalyst for water splitting. Sun et al. [12] first synthesized freestanding SnS₂ single layers with three atom thickness by liquid exfoliation. The SnS₂ single layers displayed excellent structural stability and increased density of states at the valence band edge, which achieved efficient visible light water splitting. Further, a series of regular hexagon-shaped SnS₂ nanoplates were fabricated via a facile hydrothermal process by Fu et al. [16]. The SnS₂ nanoplate-like products can efficiently delay photogenerated charge recombination, which showed good photocatalytic activity for H₂ production. Moreover, Meng and co-workers [14] reported improved

photoelectrochemical water splitting based on doped SnS₂ nanosheet arrays with amorphization, vacancy, and gradient energy band through a hydrothermal method. Taking the above reports, SnS₂ plays a key role in enhancing the visible light photocatalytic of water splitting. In this work, we reported the facile synthesis of super-thin SnS₂ nanostructure via hydrothermal and solution etching method and applied it to light-assisted electrochemical water splitting. It is expected to exhibit better performance in light-assisted electrochemical water splitting.

2. Experimental Details

2.1. Preparation of SnS₂ Nanostructure

All chemical reagents were of analytical grade and were used without further purification. SnCl₄·5H₂O, thiourea, and sulfur ammonia were purchased from Aladdin Industrial Corporation.

In the typical experiment, SnS₂ nanostructure was synthesized by the solvothermal and etching solution methods. Briefly, 0.1753 g of SnCl₄·5H₂O and 0.0952 g of thiourea were dissolved in 30 mL of ethylene glycol by ultrasound to give a transparent solution. The mixture was then transferred into a Teflon-lined autoclave (50 mL) in an oven at 180 °C for 24 h. After cooling to room temperature, the precipitate was collected from the solution through centrifugal filtration, followed by washing several times using distilled water to remove the organic residues, and dried at 60 °C for 6 h. Next, the SnS/SnS₂ heterojunctions were obtained by heat treatment at 500 °C for 30 min under Ar atmosphere. Finally, in order to obtain the SnS₂ nanostructure by the etching solution method with sulfur ammonia for 20 min (10 and 30 min), the sample was washed several times using distilled water, and dried at 60 °C.

2.2. Materials Characterizations

Sample morphology was studied by a field-emission scanning electron microscope (FESEM; FE-SEM; JSM-7000F, JEOL Ltd., Tokyo, Japan). Transmission electron microscopy (TEM) and high-resolution transmission electron microscopy (HRTEM) images were obtained using a JEOL model JEM2100 instrument at an accelerating voltage of 200 kV (JEOL Ltd., Tokyo, Japan). The crystal phase properties of the samples were analyzed with a Bruker D8 Advance X-ray diffractometer (XRD) using Ni-filtered Cu K α radiation at 40 kV, 40 mA and 2 θ range from 10° to 60° with a scan rate of 0.1° per second (Bruker Daltonics Inc., Karlsruhe, Germany). Raman spectra were obtained using a Raman spectrometer (JY T64000) excited by the 488 nm line of an Ar⁺ laser under 22 mW (HORIBA, Ltd., Kyoto, Japan). Atomic force microscopy (AFM) images were taken by Cypher S microscopy (Oxford Instruments Asylum Research, California, USA). X-ray photoelectron spectroscopy (XPS) analysis (PHI5000 Versaprobe) was used to determine the chemical composition of the products (Ulvac-Phi Inc., Kanagawa, Japan).

2.3. Light-Assisted Electrochemical Water Splitting Measurements

Light-assisted electrocatalytic activity was measured at 25 °C in a three-electrode cell connected to a CHI-760E workstation (CH Instruments, Chenhua Co., Shanghai, China). SnS₂ nanostructure (10 mg) (SnS₂ and SnS/SnS₂ heterojunction), acetylene carbon (1 mg), and 5 % polyvinylidene fluoride dimethylformamide solution (20 mg) were all mixed together. The obtained slurry was then coated onto carbon paper and then dried to form a thin-film electrode which was used as the working electrode. Meanwhile, Ag/AgCl (KCl filled) and a platinum wire both served as reference and counter electrodes, respectively. A 0.5 mol·L⁻¹ H₂SO₄ solution was used as an electrolyte. The cell geometry is dual channel electrolytic cell. A 300 W Xe lamp served as a light source in the light-assisted electrochemical water splitting measurements. The lamp provided directional light with uniform intensity distribution and was filtered to simulate the solar spectrum before illuminating the sample. Polarization curves at a scan rate of 5 mV·s⁻¹ were conducted in the above H₂SO₄ solution between 0 and -1 V. The light-assisted

electrochemical water splitting performance of SnS₂ nanosheet and SnS/SnS₂ heterojunction were also measured by the same method.

3. Results and Discussion

SnS/SnS₂ heterojunction could be synthesized through the hydrothermal and low-temperature annealing method. Then, the super-thin SnS₂ nanostructure was obtained by the reaction between SnS/SnS₂ heterojunction with ammonium persulfide. The conversion reactions:



As the ammonium persulfide solution reacted only with tin sulfide (from reaction (1)), the tin disulfide was retained. Because ammonium persulfide has poor stability at room temperature, some of the ammonium persulfides may be converted to ammonium sulfide (from reaction (3)) during the reaction. The tin sulfide will continue to react with ammonium sulfide (from reaction (2)). Therefore, samples with different morphologies can be obtained with different reaction times. From scanning electron microscopy (SEM), it was found that the mechanism was proved correct (see below). Therefore, the super-thin SnS₂ nanostructure showed a thinner thickness and a smaller size and exhibited excellent light-assisted electrochemical water splitting performance. As shown in Figures A1a and 1a, the X-ray diffraction (XRD) patterns of SnS₂ nanosheet, SnS/SnS₂ heterojunction nanosheet and super-thin SnS₂ nanostructure samples were well crystallized. Moreover, all diffraction peaks of samples were very sharp, which indicated a high crystallinity. It was observed that diffraction peaks of the super-thin SnS₂ nanostructure at 15.2, 28.2, 32.1, 41.9, 50.0, and 52.5° can be assigned to the (001), (100), (101), (102), (110), and (111) planes, respectively. Compared with SnS₂ nanosheet and SnS/SnS₂ heterojunction nanosheet (Figure A1a), we found that all the diffraction peaks of the super-thin SnS₂ nanostructure were indexed to the hexagonal SnS₂ (JCPDS No. 23-0677) [17–19]. In addition, it was found that there are no impurity peaks in the figures, indicating that the SnS₂ material was obtained after solution etching. Furthermore, in order to demonstrate the sample was the super-thin SnS₂ nanostructure after solution etching, the Raman analyzer was used to study the chemical structure (Figures A1b and 1b). From the spectra in Figure A1b, the peaks of Raman spectra at 182, 220, and 312 cm⁻¹ were SnS and SnS₂, respectively. And Figure 1b shows the Raman spectra of the super-thin SnS₂ nanostructure. The peak at 312.1 cm⁻¹ was matched well with hexagonal SnS₂ [20–22].

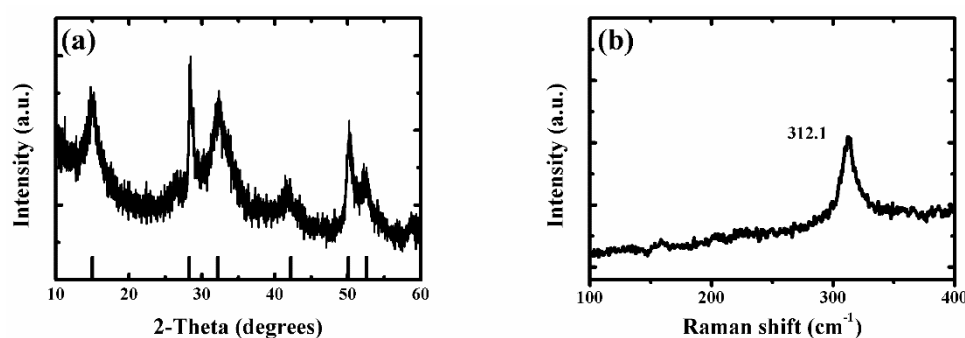


Figure 1. (a) The typical XRD pattern of the super-thin SnS₂ nanostructure. (b) The typical Raman spectra of the super-thin SnS₂ nanostructure.

Moreover, Figures 2, A2 and A3 show the field-emission scanning electron microscopy (FESEM) and transmission electron microscopy (TEM) images of the super-thin SnS₂ nanostructure. The typical FESEM image of the super-thin SnS₂ nanostructure displayed a typical super-thin nanosheet

morphology. Moreover, in contrast with the FESEM of the SnS₂ nanosheet and SnS/SnS₂ heterojunction nanosheet in Figure A2, the super-thin SnS₂ nanostructure showed the thinner nanostructure. This super-thin nanostructure could improve fast carrier transport and greatly reduce the recombination rate [12,23,24]. Figure 2b reveals the FESEM and energy-dispersive spectrometry (EDS) of the super-thin SnS₂ nanostructure, the elemental mapping images confirm that the elements Sn and S were uniformly distributed among the sample [25,26]. Moreover, Figure A3 also shows the elements were uniformly distributed in the samples by the different time of solution etching. The uniform morphologies of the super-thin SnS₂ nanostructure were also investigated by the TEM in Figure 2c,d. The super-thin SnS₂ nanostructure with a lateral size of about 1 μm was observed. Additionally, the high-resolution transmission electron microscopy (HRTEM) image taken from the selected area in Figure 1c is shown in Figure 1d, which exhibited a crystal lattice spacing of 0.28 nm and belonged to the crystal facet (101) of hexagonal SnS₂ [19,27,28]. Figure 2e,f shows the atomic force microscope (AFM) images of the SnS₂ nanosheet and super-thin SnS₂ nanostructure, which can further characterize the size and morphology. Figure 2f shows the super-thin SnS₂ nanostructure with a thickness of 1.7 nm and lateral dimension of ~ 250 nm. Due to the above results, the super-thin SnS₂ nanostructure showed a thinner nanostructure and a larger specific surface area than the SnS₂ nanosheet. Therefore, the super-thin SnS₂ nanostructure would exhibit excellent light-assisted electrochemical activity performance.

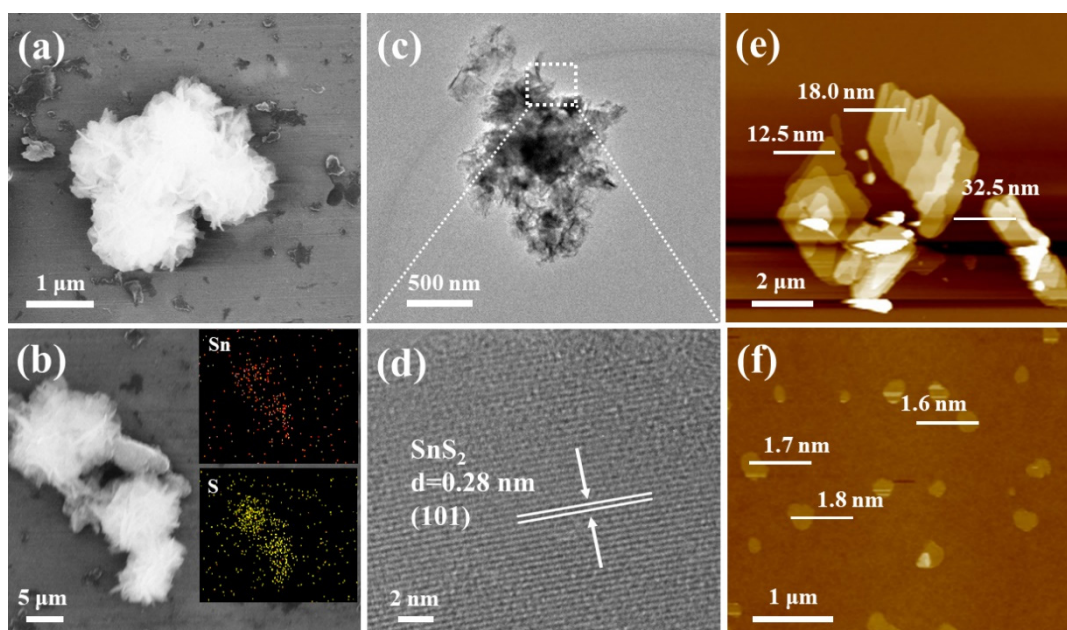


Figure 2. (a) The typical field-emission scanning electron microscope (FESEM) image of the super-thin SnS₂ nanostructure. (b) The typical FESEM image and the energy-dispersive spectrometry (EDS) of the super-thin SnS₂ nanostructure. (c) The typical transmission electron microscopy (TEM) image of the super-thin SnS₂ nanostructure. (d) The typical high-resolution transmission electron microscopy (HRTEM) image of the super-thin SnS₂ nanostructure, (e,f) atomic force microscopy (AFM) image of SnS₂ nanosheet and super-thin SnS₂ nanostructure.

To further confirm the surface-chemical states of the super-thin SnS₂ nanostructure, the X-ray photoelectron spectroscopy (XPS) spectra were characterized in Figure 3. Figure 3a shows the wide scan spectrum of the super-thin SnS₂ nanostructure, the Sn, S, C, and O elements were detected. It was indicated that the sample contained those elements and no other impurities could be found. The peaks at 495.2 and 486.6 eV were observed in Figure 3b, which was recognized as the 3d_{3/2} and 3d_{5/2} states of Sn⁴⁺ for the hexagonal SnS₂ [8,14]. Moreover, the high-resolution XPS spectra for S 2p can be fitted with two peaks of 164.3 and 163.0 eV, corresponding to 2p_{1/2} and 2p_{3/2} states of S²⁻, respectively [29–31].

From the XRD, Raman, FESEM, TEM, and XPS data representation, the super-thin SnS₂ nanostructure was successfully fabricated through the hydrothermal and solution etching method.

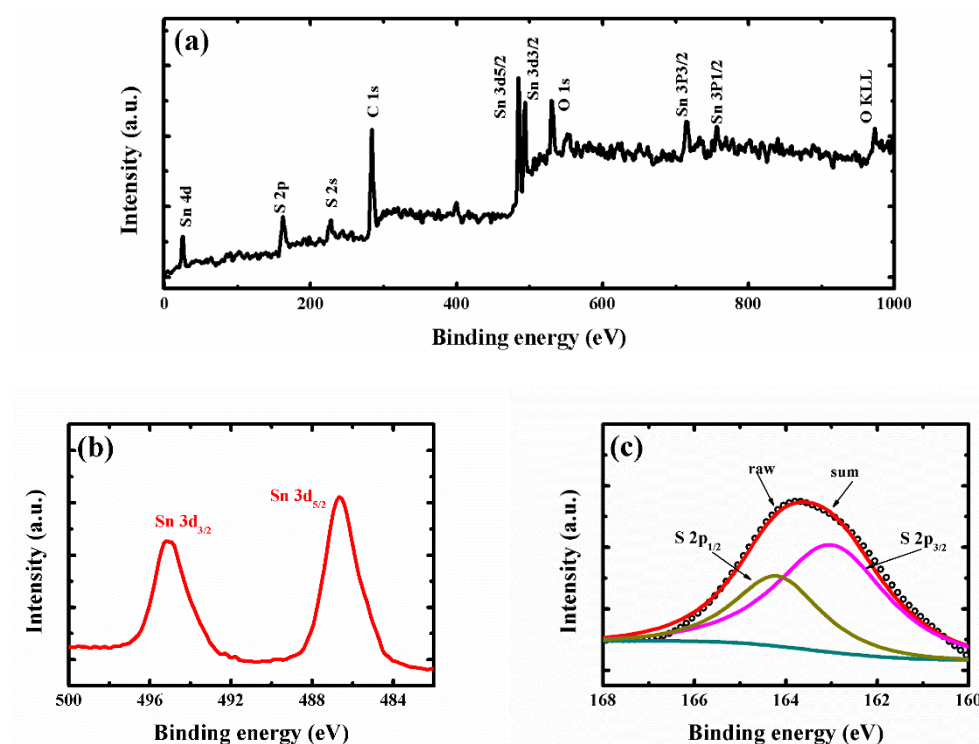


Figure 3. (a) Full XPS spectrum of the super-thin SnS₂ nanostructure. (b) High-resolution XPS spectra of Sn 3d. (c) High resolution XPS spectra of S 2p.

To evaluate the light-assisted electrochemical water splitting performance, the super-thin SnS₂ nanostructure, SnS₂ nanosheet, and SnS/SnS₂ heterojunction sheet were measured by the typical three-electrode cell connected with a CHI 670E configuration in 0.5 M H₂SO₄ solution under a 300 W Xe lamp at the room temperature [14,16,32–35]. Figure 4a shows the linear sweep voltammetry (LSV) curves of the samples. The SnS₂ nanosheet displayed poorer photocatalytic activity than the SnS/SnS₂ heterojunction sheet. SnS/SnS₂ heterojunction sheet showed improved light-assisted electrochemical water splitting performance, which depended on its specific energy band structure (Figure A4 shows that the photo-generated electrons on the CB of SnS can easily flow to the CB of SnS₂ through the interface. In the same way, the holes on the VB of SnS₂ are more positive than those of SnS and can be transferred to the VB of SnS and the VB edge level of SnS₂. It can be efficient electron-hole pair separation and enhance photocatalytic activity). However, the super-thin SnS₂ nanostructure displayed an overpotential of 0.25 V at the current density of -10 mA cm^{-2} , which exhibited better overpotential than the SnS₂ nanosheet and SnS/SnS₂ heterojunction sheet and proved its superior hydrogen evolution reaction (HER) activity by the higher electrochemically active surface areas (Figures 4c and A7). Meanwhile, to check the durability of the super-thin SnS₂ nanostructure, the basically unchanged LSV curves can be observed from comparing before and after 1000 cycles. Additionally, as the as-prepared SnS₂ nanostructures were further compared with different times of solution etching, the samples were also analyzed by the LSV curves under the same conditions in Figure A5. The sample with 20 min solution etching (super-thin SnS₂ nanostructure) displayed the best HER performance of all samples (solution etching 10 and 30 min). Therefore, the electrochemically active surface areas (ECSA) of the super-thin SnS₂ nanostructure, SnS₂ nanosheet and SnS/SnS₂ heterojunction sheet were measured by the double-layer capacitances (C_{dl}). The C_{dl} was estimated through the investigated cycling voltammetry (CV) curves at different scan rates under non-faradaic region (Figure A6). As shown in Figure 4c, the super-thin SnS₂ nanostructure exhibited larger C_{dl} value than that of SnS₂ nanosheet

and SnS/SnS₂ heterojunction sheet. Interestingly, the super-thin SnS₂ nanostructure exhibited larger ECSA than SnS₂ nanosheet, which was regarded as higher catalytic activity. Moreover, better intrinsic catalytic activity for super-thin SnS₂ nanostructure was further proved by its ECSA-corrected current densities in comparison with SnS₂ nanosheet and SnS/SnS₂ heterojunction in Figure A7 (detailed discussion in Appendix A). Due to the above results, the super-thin SnS₂ nanostructure has a higher active surface area and more active sites, which can enhance HER property.

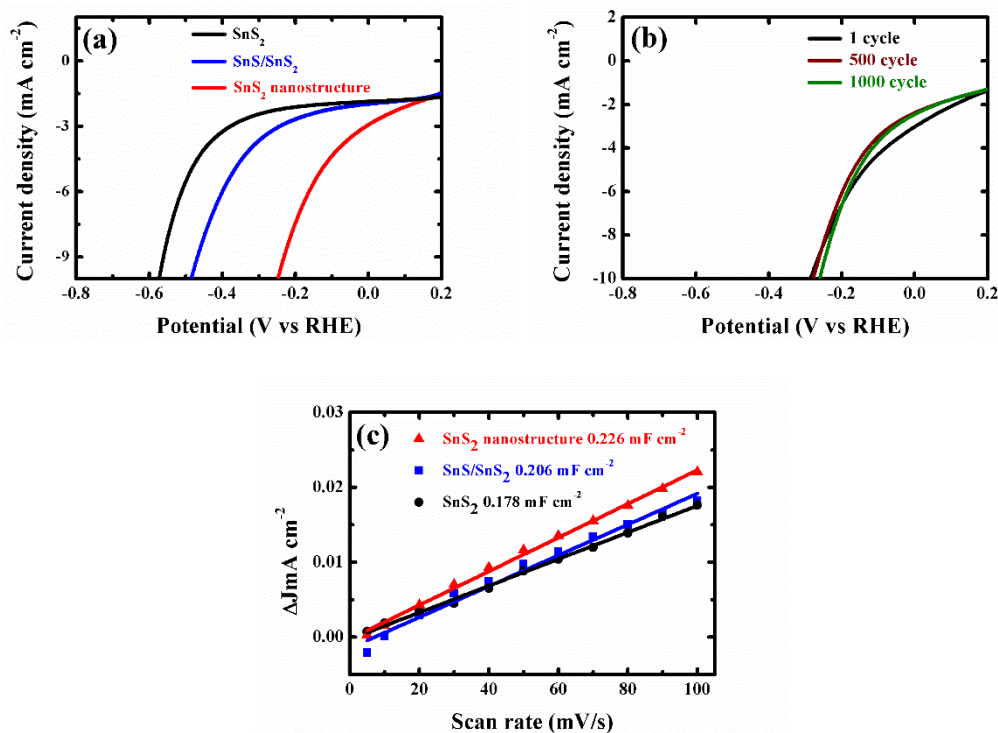


Figure 4. (a) Linear sweep voltammetry (LSV) curves of the SnS₂ nanosheets, SnS/SnS₂ heterojunction and super-thin SnS₂ nanostructure for hydrogen evolution reaction (HER) in 0.5 M H₂SO₄ solution. (b) LSV curves of the super-thin SnS₂ nanostructure before and after 1000 cycles. (c) The capacitive currents at -0.05 V as a function of scan rate for SnS₂ nanosheets, SnS/SnS₂ heterojunction and super-thin SnS₂ nanostructure.

4. Conclusions

In summary, the super-thin SnS₂ nanostructure has been successfully synthesized through a hydrothermal and solution etching route. The super-thin SnS₂ nanostructure offered excellent light-assisted electrochemical water splitting performance due to effectively capturing visible light, enhancing carrier density, rapid charge transfer and fast chemical reaction. Given these unique benefits, we believe that super-thin SnS₂ nanostructure built on the other trend can provide a new potential application for electrochemical/photo-electrocatalytic devices.

Author Contributions: The experiments and characterizations were carried out by H.S., with the assistance of H.W., Y.G., K.W. and X.S. under the guidance of S.Y. and Y.S., H.S. and S.Y. wrote the manuscript and prepared all figures. Y.S. and S.Y. supervised and coordinated all the work.

Acknowledgments: This work is supported by the National Basic Research Program of China (973 Program: 2018YFA0209101), the National Science Foundations of China (No. 61205057, No. 11574136).

Conflicts of Interest: The authors declare no conflict of interest.

Appendix A

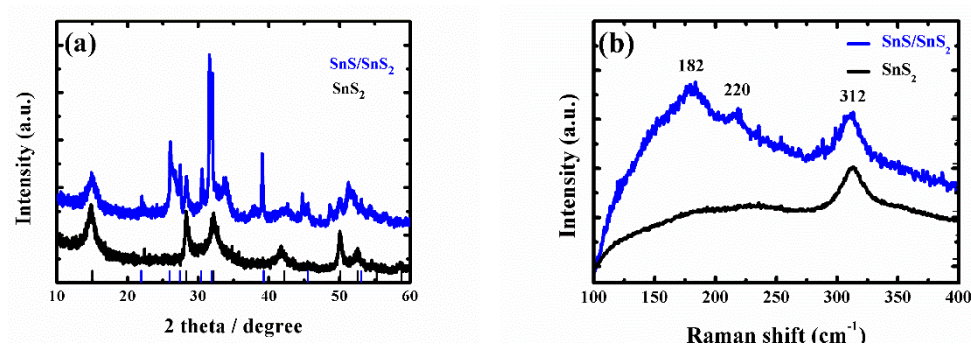


Figure A1. (a) XRD pattern of the SnS₂ nanosheets and SnS/SnS₂ heterojunction. (b) Raman spectra of the SnS₂ nanosheets and SnS/SnS₂ heterojunction.

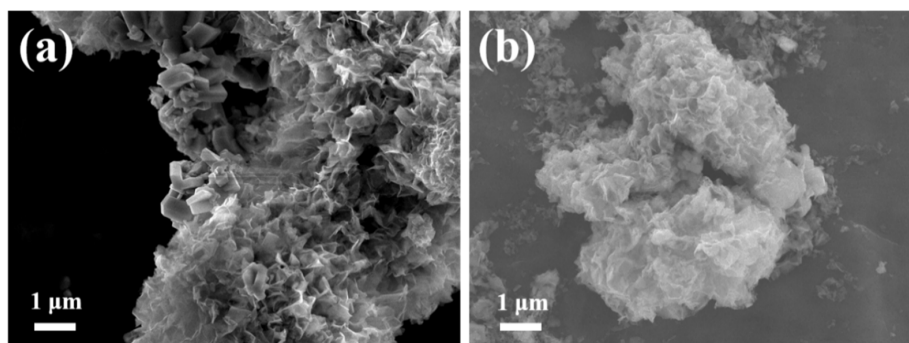


Figure A2. (a) The FESEM of the SnS₂ nanosheets, (b) the FESEM of the SnS/SnS₂ heterojunction.

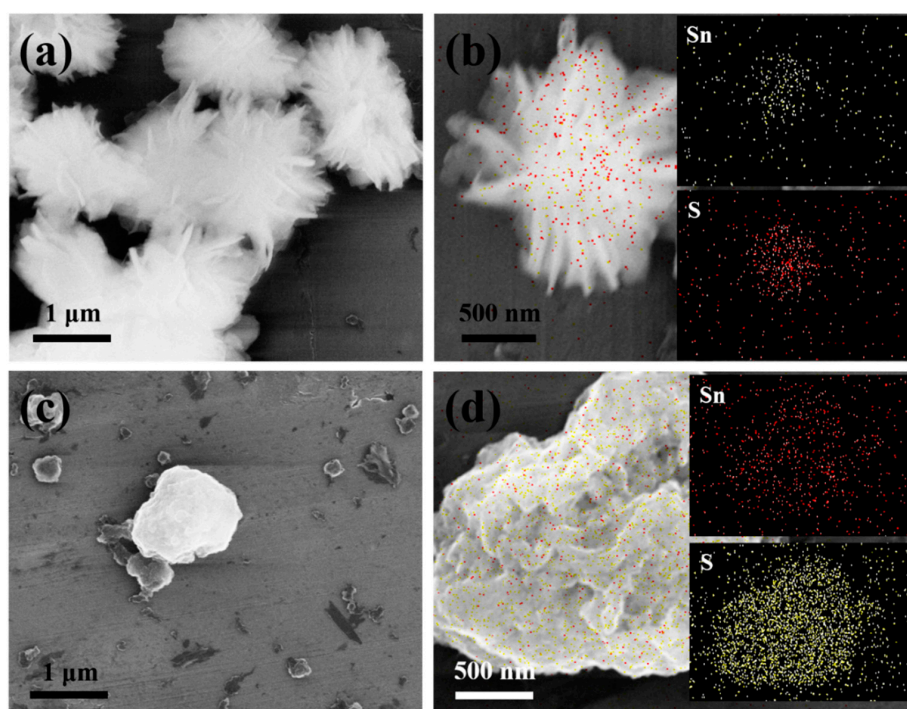


Figure A3. (a) The FESEM image of the SnS₂ nanosheet with solution etching 10 min. (b) The FESEM image and EDS of the SnS₂ nanosheet with solution etching 10 min. (c) The FESEM image of the SnS₂ nanosheet with solution etching 30 min. (d) The FESEM image and EDS of the SnS₂ nanosheet with solution etching 30 min.

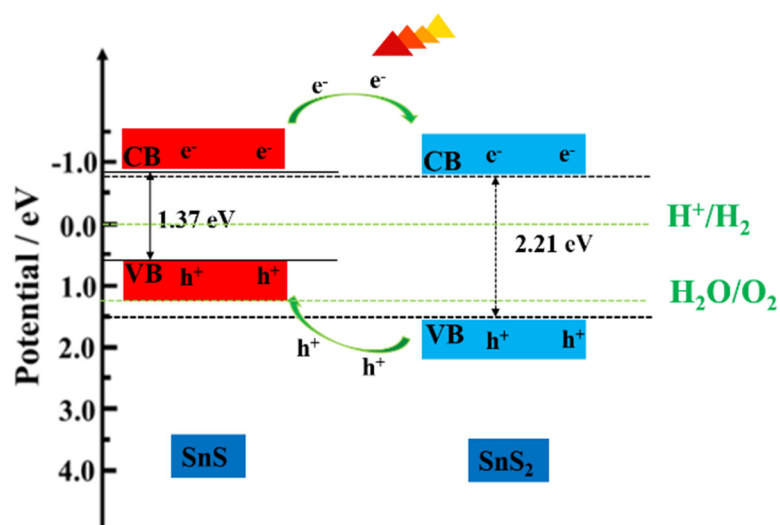


Figure A4. Schematic diagram for energy band matching and electron-hole separations.

The SnS/SnS₂ heterojunction nanosheet acts as a photocathode, the catalytic mechanisms may be responsible for the following reasons: As shown in Figure A5, when SnS₂ is in contact with SnS to form p-n heterostructure, these photo-generated electrons on the CB of SnS can easily flow to the CB of SnS₂ through the interface. It is considered that the CB position of SnS is more negative than the CB position of SnS₂. In the same way, the holes on the VB of SnS₂ tend to transfer to the VB of SnS and the VB edge level of SnS₂ is more positive than that of SnS, which can cause efficient electron-hole pair separation and thus lead to enhanced photocatalytic activity.

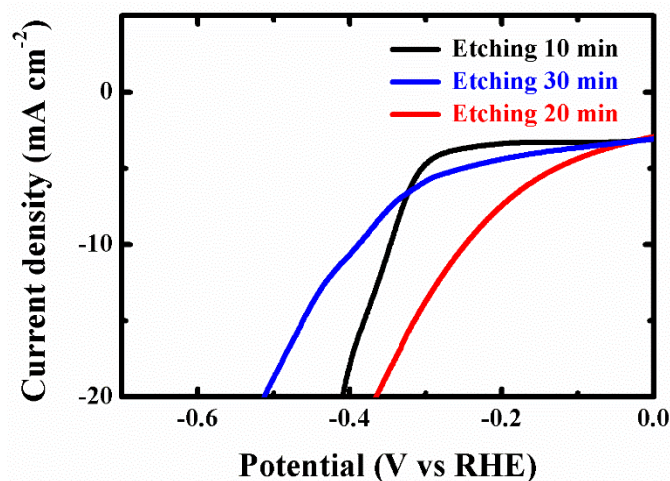


Figure A5. LSV curves of the SnS₂ nanosheet by solution etching 10, 20, and 30 min with HER in 0.5 M H₂SO₄ solution.

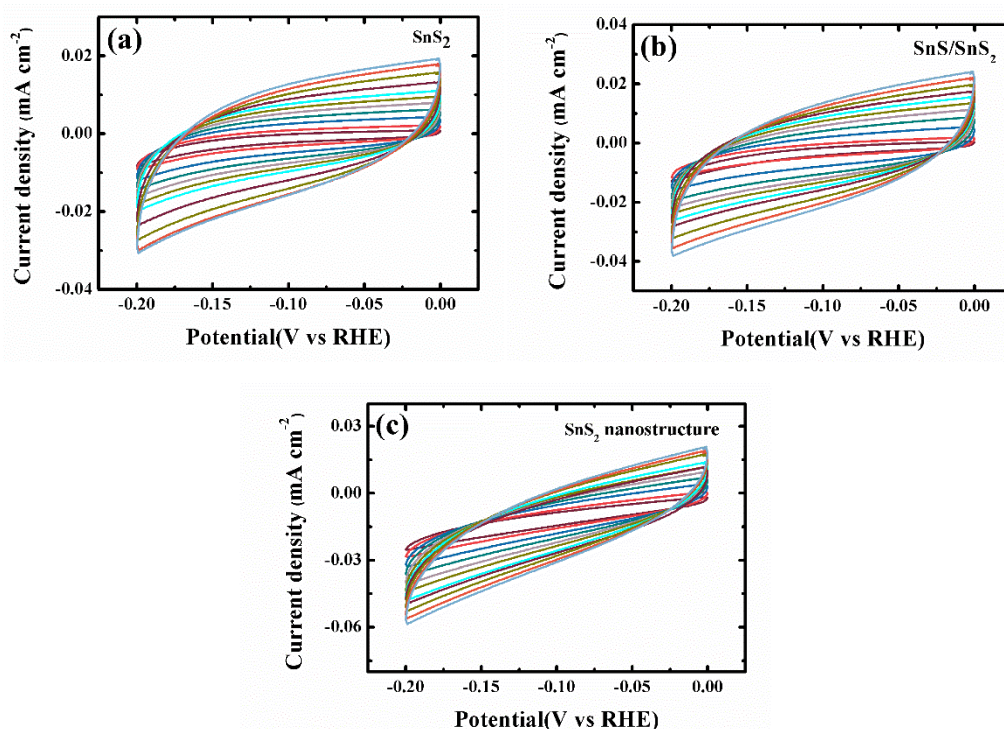


Figure A6. Cyclic voltammograms of (a) SnS₂ nanosheets, (b) SnS/SnS₂ heterojunction and (c) SnS₂ nanostructure were measured in the non-faradaic capacitance current range at scan rates of 5, 10, 20, 30, 40, 50, 60, 70, 80, 90, and 100 mV s⁻¹.

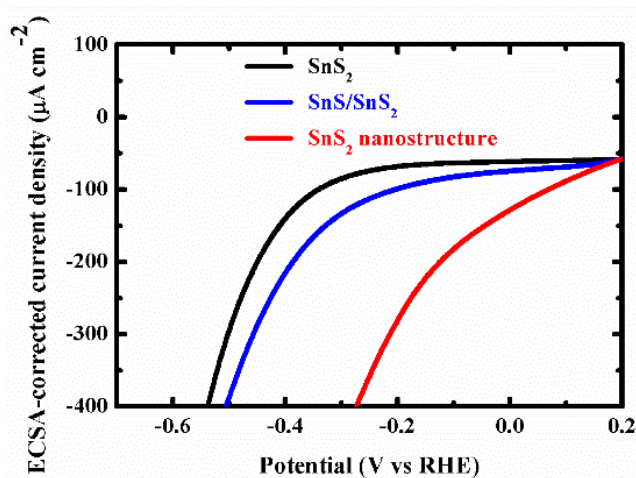


Figure A7. ECSA-corrected current densities versus applied potentials.

To measure electrochemical double-layer capacitance (Cdl), the potential was swept nine times at each scan rate (5, 10, 20, 30, 40, 50, 60, 70, 80, 90, and 100 mV/s) in the scan range from -0.20 to 0 V vs. RHE. Capacitive currents were measured in a potential range where no faradic processes were observed. The measured capacitive currents difference (ΔJ) at -0.05 V vs. RHE was plotted against scan rate and specific capacitance was determined from the slope of the linear fitting. The Cdl values for SnS₂ nanosheet and SnS/SnS₂ heterojunction sheet and super-thin SnS₂ nanostructure are calculated to be 0.178, 0.206, and 0.226 mF·cm⁻², respectively. The specific capacitance is converted into an electrochemical surface area (ECSA) using the specific capacitance value for a flat standard with 1 cm² of real surface area. We use the specific capacitance (20–60 $\mu\text{F cm}^{-2}$) of 40 $\mu\text{F cm}^{-2}$ here to calculate the ECSA (Nature Communications, 2018, 9, 2452. and Nature Communications, 2019, 10, 399.) according to Equation (A1):

$$ECSA = \frac{C_{dl}}{40 \mu F/cm^2} cm^2_{ECSA} \quad (A1)$$

Calculated electrochemical active surface area:

SnS₂ sheet:

$$A_{ECSA}^{SnS_2} = \frac{0.178 mF cm^{-2}}{40 \mu F cm^{-2} per cm^2_{ECSA}} = 4.45 cm^2_{ECSA} \quad (A2)$$

SnS/SnS₂ heterojunction sheet:

$$A_{ECSA}^{SnS/SnS_2} = \frac{0.206 mF cm^{-2}}{40 \mu F cm^{-2} per cm^2_{ECSA}} = 5.15 cm^2_{ECSA} \quad (A3)$$

Super-thin SnS₂ nanostructure:

$$A_{ECSA}^{S-SnS_2} = \frac{0.226 mF cm^{-2}}{40 \mu F cm^{-2} per cm^2_{ECSA}} = 5.65 cm^2_{ECSA} \quad (A4)$$

References

1. Wang, Y.; Kim, J.C.; Wu, R.J.; Martinez, J.; Song, X.; Yang, J.; Zhao, F.; Mkhoyan, A.; Jeong, H.Y.; Chhowalla, M. Van der Waals contacts between three-dimensional metals and two-dimensional semiconductors. *Nature* **2019**, *568*, 70–74. [[CrossRef](#)] [[PubMed](#)]
2. Illarionov, Y.Y.; Bانشchikov, A.G.; Polyushkin, D.K.; Wachter, S.; Knobloch, T.; Thesberg, M.; Mennel, L.; Paur, M.; Stöger-Pollach, M.; Steiger-Thirsfeld, A.; et al. Ultrathin calcium fluoride insulators for two-dimensional field-effect transistors. *Nat. Electron.* **2019**, *2*, 230–235. [[CrossRef](#)]
3. Yin, J.; Tan, Z.; Hong, H.; Wu, J.; Yuan, H.; Liu, Y.; Chen, C.; Tan, C.; Yao, F.; Li, T. Ultrafast and highly sensitive infrared photodetectors based on two-dimensional oxyselenide crystals. *Nat. Commun.* **2018**, *9*, 3311. [[CrossRef](#)] [[PubMed](#)]
4. Konstantatos, G. Current status and technological prospect of photodetectors based on two-dimensional materials. *Nat. Commun.* **2018**, *9*, 5266. [[CrossRef](#)] [[PubMed](#)]
5. Liu, G.; Zhen, C.; Kang, Y.; Wang, L.; Cheng, H.M. Unique physicochemical properties of two-dimensional light absorbers facilitating photocatalysis. *Chem. Soc. Rev.* **2018**, *47*, 6410–6444. [[CrossRef](#)]
6. Chen, C.; Xie, X.; Anasori, B.; Sarycheva, A.; Makaryan, T.; Zhao, M.; Urbankowski, P.; Miao, L.; Jiang, J.; Gogotsi, Y. MoS₂-on-MXene heterostructures as highly reversible anode materials for lithium-ion batteries. *Angew. Chem. Int. Ed.* **2018**, *57*, 1846–1850. [[CrossRef](#)] [[PubMed](#)]
7. Yan, S.; Wang, B.; Wang, Z.; Hu, D.; Xu, X.; Wang, J.; Shi, Y. Supercritical carbon dioxide-assisted rapid synthesis of few-layer black phosphorus for hydrogen peroxide sensing. *Biosens. Bioelectron.* **2016**, *80*, 34–38. [[CrossRef](#)]
8. Khan, Z.; Parveen, N.; Ansari, S.A.; Senthilkumar, S.T.; Park, S.; Kim, Y.; Cho, M.H.; Ko, H. Three-dimensional SnS₂ nanopetals for hybrid sodium-air batteries. *Electrochim. Acta* **2017**, *257*, 328–334. [[CrossRef](#)]
9. Khan, Z.; Park, S.; Hwang, S.M.; Yang, J.; Lee, Y.; Song, H.K.; Kim, Y.; Ko, H. Hierarchical urchin-shaped α-MnO₂ on graphene-coated carbon microfibers: A binder-free electrode for rechargeable aqueous Na-air battery. *NPG Asia Mater.* **2016**, *8*, e294. [[CrossRef](#)]
10. Liu, Y.; Wang, J.; Kim, S.; Sun, H.; Yang, F.; Fang, Z.; Tamura, N.; Zhang, R.; Song, X.; Wen, J. Helical van der Waals crystals with discretized Eshelby twist. *Nature* **2019**, *570*, 358–362. [[CrossRef](#)]
11. Lin, S.; Carvalho, A.; Yan, S.; Li, R.; Kim, S.; Rodin, A.; Carvalho, L.; Chan, E.M.; Wang, X.; Neto, A.H.C.; et al. Accessing valley degree of freedom in bulk Tin (II) sulfide at room temperature. *Nat. Commun.* **2018**, *9*, 1455. [[CrossRef](#)] [[PubMed](#)]
12. Sun, Y.; Cheng, H.; Gao, S.; Sun, Z.; Liu, Q.; Liu, Q.; Lei, F.; Yao, T.; He, J.; Wei, S.; et al. Freestanding tin disulfide single-layers realizing efficient visible-light water splitting. *Angew. Chem. Int. Ed.* **2012**, *51*, 8727–8731. [[CrossRef](#)] [[PubMed](#)]
13. Zhang, Y.C.; Du, Z.N.; Li, S.Y.; Zhang, M. Novel synthesis and high visible light photocatalytic activity of SnS₂ nanoflakes from SnCl₂·2H₂O and S powders. *Appl. Catal. B Environ.* **2010**, *95*, 153–159. [[CrossRef](#)]

14. Meng, L.; Wang, S.; Cao, F.; Tian, W.; Long, R.; Li, L. Doping-Induced Amorphization, Vacancy, and Gradient Energy Band in SnS₂ Nanosheet Arrays for Improved Photoelectrochemical Water Splitting. *Angew. Chem. Int. Ed.* **2019**, *58*, 6761–6765. [[CrossRef](#)] [[PubMed](#)]
15. Giri, B.; Masroor, M.; Yan, T.; Kushnir, K.; Carl, A.D.; Doiron, C.; Zhang, H.; Zhao, Y.; McClelland, A.; Tompsett, G.A. Balancing Light Absorption and Charge Transport in Vertical SnS₂ Nanoflake Photoanodes with Stepped Layers and Large Intrinsic Mobility. *Adv. Energy Mater.* **2019**, *9*, 1901236. [[CrossRef](#)]
16. Fu, W.; Wang, J.; Zhou, S.; Li, R.; Peng, T. Controllable fabrication of regular hexagon-shaped SnS₂ nanoplates and their enhanced visible-light-driven H₂ production activity. *ACS Appl. Nano Mater.* **2018**, *1*, 2923–2933. [[CrossRef](#)]
17. Tu, F.; Xu, X.; Wang, P.; Si, L.; Zhou, X.; Bao, J. A few-layer SnS₂/reduced graphene oxide sandwich hybrid for efficient sodium storage. *J. Phys. Chem. C* **2017**, *121*, 3261–3269. [[CrossRef](#)]
18. Jiang, Y.; Wei, M.; Feng, J.; Ma, Y.; Xiong, S. Enhancing the cycling stability of Na-ion batteries by bonding SnS₂ ultrafine nanocrystals on amino-functionalized graphene hybrid nanosheets. *Energy Environ. Sci.* **2016**, *9*, 1430–1438. [[CrossRef](#)]
19. Yan, S.; Li, K.; Lin, Z.; Song, H.; Jiang, T.; Wu, J.; Shi, Y. Fabrication of a reversible SnS₂/RGO nanocomposite for high performance lithium storage. *RSC Adv.* **2016**, *6*, 32414–32421. [[CrossRef](#)]
20. Gong, Y.; Yuan, H.; Wu, C.L.; Tang, P.; Yang, S.Z.; Yang, A.; Li, G.; Liu, B.; van de Groep, J.; Brongersma, M. Spatially controlled doping of two-dimensional SnS₂ through intercalation for electronics. *Nat. Nanotechnol.* **2018**, *13*, 294–299. [[CrossRef](#)]
21. Li, Q.; Wei, A.; Guo, Z.; Liu, J.; Zhao, Y.; Xiao, Z. Chemical vapor deposition of two-dimensional SnS₂ nanoflakes and flower-shaped SnS₂. *J. Mater. Sci. Mater. Electron.* **2018**, *29*, 16057–16063. [[CrossRef](#)]
22. Wang, S. Solvothermal synthesis of porous SnS₂ nanotubes with higher adsorption and photocatalytic activity. *Surf. Sci.* **2019**, *690*, 121469. [[CrossRef](#)]
23. Song, F.; Hu, X. Exfoliation of layered double hydroxides for enhanced oxygen evolution catalysis. *Nat. Commun.* **2014**, *5*, 4477. [[CrossRef](#)] [[PubMed](#)]
24. Yu, J.; Xu, C.Y.; Ma, F.X.; Hu, S.P.; Zhang, Y.W.; Zhen, L. Monodisperse SnS₂ nanosheets for high-performance photocatalytic hydrogen generation. *ACS Appl. Mater. Interfaces* **2014**, *6*, 22370–22377. [[CrossRef](#)] [[PubMed](#)]
25. Liu, J.; Wang, J.; Zhang, B.; Ruan, Y.; Wan, H.; Ji, X.; Xu, K.; Zha, D.; Miao, L.; Jiang, J. Mutually beneficial Co₃O₄@MoS₂ heterostructures as a highly efficient bifunctional catalyst for electrochemical overall water splitting. *J. Mater. Chem. A* **2018**, *6*, 2067–2072. [[CrossRef](#)]
26. Wang, J.; Luo, C.; Mao, J.; Zhu, Y.; Fan, X.; Gao, T.; Mignerey, A.C.; Wang, C. Solid-State Fabrication of SnS₂/C Nanospheres for High-Performance Sodium Ion Battery Anode. *ACS Appl. Mater. Interfaces* **2015**, *7*, 11476–11481. [[CrossRef](#)] [[PubMed](#)]
27. Jing, X.; Li, L.; Xie, J.; Yan, H.; Yuan, Y.; Chen, M.; Cheng, H.; Yue, Z.; Su, N.; Wang, X. Layer-by-layered SnS₂/graphene hybrid nanosheets via ball-milling as promising anode materials for lithium ion batteries. *Electrochim. Acta* **2018**, *269*, 452–461.
28. Wu, Y.; Nie, P.; Wu, L.; Dou, H.; Zhang, X. 2D MXene/SnS₂ composites as high-performance anodes for sodium ion batteries. *Chem. Eng. J.* **2018**, *334*, 932–938. [[CrossRef](#)]
29. Xie, Y.; Fan, M.; Shen, T.; Liu, Q.; Chen, Y. SnS₂ nanoplates as stable anodes for sodium ion and lithium ion batteries. *Mater. Technol.: Adv. Perform. Mater.* **2016**, *31*, 646–652. [[CrossRef](#)]
30. Li, K.; Yan, S.; Lin, Z.; Dai, X.; Qu, P. Preparation and lithium ion batteries properties of SnS₂ nanoparticle/reduced graphene oxide nanosheet nanocomposites using supercritical carbon dioxide. *Synth. Met.* **2016**, *217*, 138–143. [[CrossRef](#)]
31. Khan, Z.; Park, S.O.; Yang, J.; Park, S.; Shanker, R.; Song, H.K.; Kim, Y.; Kwak, S.K.; Ko, H. Binary N, S-doped carbon nanospheres from bio-inspired artificial melanosomes: A route to efficient air electrodes for seawater batteries. *J. Mater. Chem. A* **2018**, *6*, 24459–24467. [[CrossRef](#)]
32. Jarne, C.; Paul, L.; Conesa, J.C.; Shleev, S.; De Lacey, A.L.; Pita, M. Underpotential Photoelectrooxidation of Water by SnS₂-Laccase Co-catalysts on Nanostructured Electrodes with Only Visible-Light Irradiation. *ChemElectroChem* **2019**, *6*, 2755–2761. [[CrossRef](#)]
33. Huang, P.C.; Shen, Y.M.; Brahma, S.; Shaikh, M.O.; Huang, J.L.; Wang, S.C. SnS_x (x = 1, 2) nanocrystals as effective catalysts for photoelectrochemical water splitting. *Catalysts* **2017**, *7*, 252. [[CrossRef](#)]

34. Liu, E.; Chen, J.; Ma, Y.; Feng, J.; Jia, J.; Fan, J.; Hu, X. Fabrication of 2D SnS₂/g-C₃N₄ heterojunction with enhanced H₂ evolution during photocatalytic water splitting. *J. Colloid Interface Sci.* **2018**, *524*, 313–324. [[CrossRef](#)] [[PubMed](#)]
35. Zhou, G.; Shan, Y.; Wang, L.; Hu, Y.; Guo, J.; Hu, F.; Shen, J.; Gu, Y.; Cui, J.; Liu, L.; et al. Photoinduced semiconductor-metal transition in ultrathin troilite FeS nanosheets to trigger efficient hydrogen evolution. *Nat. Commun.* **2019**, *10*, 399. [[CrossRef](#)] [[PubMed](#)]



© 2019 by the authors. Licensee MDPI, Basel, Switzerland. This article is an open access article distributed under the terms and conditions of the Creative Commons Attribution (CC BY) license (<http://creativecommons.org/licenses/by/4.0/>).